Crystal symmetry and pressure effects on the valence band structure of γ-InSe and ε-GaSe: Transport measurements and electronic structure calculations

D. Errandonea,[1,*] A. Segura,[1] F. J. Manjón,[2] A. Chevy,[3] E. Machado,[4] G. Tobias,[4] P. Ordejón,[4] and E. Canadell[4]
[1]*Departamento de Física Aplicada, ICMUV, Universitat de València, Edificio de Investigación, c/Dr. Moliner 50, 46100 Burjassot (Valencia), Spain*
[2]*Departamento de Física Aplicada, Universitat Politécnica de València, EPSA, 03801 Alcoi, Spain*
[3]*Physique des Milieux Condenses, Universite Pierre et Marie Curie, 75252 Paris, Cedex 05, France*
[4]*Institut de Ciència dels Materials de Barcelona, CSIC, Campus de la UAB, 08193 Bellaterra (Barcelona), Spain*
(Received 4 August 2004; revised manuscript received 8 October 2004; published 18 March 2005)

This paper reports on Hall effect and resistivity measurements under high pressure up to 3–4 GPa in *p*-type γ-indium selenide (InSe) (doped with As, Cd, or Zn) and ε-gallium selenide (GaSe) (doped with N or Sn). The pressure behavior of the hole concentration and mobility exhibits dramatic differences between the two layered compounds. While the hole concentration and mobility increase moderately and monotonously in ε-GaSe, a large increase of the hole concentration near 0.8 GPa and a large continuous increase of the hole mobility, which doubled its ambient pressure value by 3.2 GPa, is observed in γ-InSe. Electronic structure calculations show that the different pressure behavior of hole transport parameters can be accounted for by the evolution of the valence-band maximum in each material under compression. While the shape of the valence band maximum is virtually pressure-insensitive in ε-GaSe, it changes dramatically in γ-InSe, with the emergence of a ring-shaped subsidiary maximum that becomes the absolute valence-band maximum as pressure increases. These differences are shown to be a consequence of the presence or absence of a symmetry element (mirror plane perpendicular to the anisotropy axis) in the point group of each polytype (D_{3h} for the ε-polytype and C_{3v} for the γ-polytype), resulting in different selection rules that affect the $\vec{k}\cdot\vec{p}$ interaction between valence bands.

DOI: 10.1103/PhysRevB.71.125206 PACS number(s): 78.20.Bh

I. INTRODUCTION

The effect of the crystal symmetry on the optical, lattice, and transport properties of III-VI layered semiconductors was an object of debate and investigation for many years. The basic structure and symmetry of an isolated layer is the same (D_{3h} point group) for three of the most studied members of this family, namely indium selenide (InSe), gallium selenide (GaSe), and gallium sulfide (GaS). This similarity breaks in the bulk compounds, as each layer stacking sequence leads to a different polytype, with a different crystal symmetry: γ-polytype for InSe (C_{3v} point group),[1] ε-polytype for GaSe (D_{3h} point group)[2] and β-polytype for GaS (D_{6h} point group).[3] The effect of the polytype symmetry in the lattice dynamics is obviously very clear (through the selection rules for the Raman effect) and has been widely investigated.[4–7] By contrast, its effect in optical and transport properties is far less obvious. It is worth noticing that the absorption edges of γ-InSe and ε-GaSe exhibit virtually the same features and intensity, apart from the photon energy shift.[8–11] Even if there were some studies in the early 1970s on the polytype effect on the band gap of GaSe (Ref. 12), there was no clear trend and these suggestions have never been revisited in light of modern electronic structure calculation methods, which are far more accurate that the empirical pseudopotential methods that were used in the interpretation of the early results.

Given the amount of extrinsic parameters involved in transport properties, they do not appear as the first choice when one is looking for symmetry-based differences between polytypes. Nevertheless, transport measurements under pressure can be a very efficient tool to detect changes in the band structure. In the case of InSe, the energy difference between the indirect subsidiary minima and the direct absolute minimum of the conduction band decreases upon compression, and a direct-indirect band-gap crossover occurs at 4 GPa (Refs. 13 and 14). These changes of the conduction-band structure affect the transport properties of *n*-type InSe. Hence, research of the transport properties of *n*-type under compression[15,16] valuably contributed to the understanding of the pressure behavior of the conduction-band structure of InSe.

On the other hand, density-functional-theory (DFT) electronic structure calculations showed that the valence-band structure of InSe exhibits a complex behavior under pressure leading to a nonconventional direct-to-indirect crossover.[13,14,17,18] The valence band of InSe above 4 GPa exhibits a singular feature: a ringshaped (toroidal) constant energy surface.[14] These changes of the valence-band structure of InSe are expected to strongly affect the transport properties of *p*-type InSe. Previous results on transport measurements under pressure in *p*-type GaSe did not suggest any drastic change.[19] This fact motivated us to perform Hall effect (HE) measurements in *p*-type InSe samples doped with As, Cd, and Zn (Ref. 20) and to compare them to those previously obtained for *p*-GaSe doped with Sn and N under the light of first principles band structure calculations for both compounds.

After describing the experimental method and the band structure calculations in Sec. II, we will present the experimental results in Sec. III. The evolution of the electronic structure of both compounds under pressure will be the key

to discussing the differences between both compounds in Sec. IV.

II. EXPERIMENTAL DETAILS AND BAND STRUCTURE CALCULATION METHODS

The studies were performed in InSe and GaSe monocrystals grown by the Bridgmann method. Impurities were introduced as InAs, CdSe, or ZnSe for InSe (Ref. 21). Growth of *p*-doped GaSe has been described in Ref. 19. The HE measurements under variable pressure and temperature (T) were carried out in a Bridgmann-type cell, equipped with tungsten carbide anvils, which admits the application of an external magnetic field (0.6 T). Samples, with faces perpendicular to the *c* axis, were cleaved from large monocrystals, being typically 50 μm thick and 4×4 mm^2 in size. Contacts were applied in the van der Pauw configuration by soldering silver wires with high-purity indium. The pressure apparatus used for the experiments has been described elsewhere.[15,16,19] In this case, we used pyrophyllite gaskets, thermally treated at 950 °C during 1 hour, in the split gasket geometry (0.8 mm thick each). The quasihydrostatic pressure generated was estimated from pressure calibrations based on resistance changes[22] The pressure cell was heated with a nichrome heater placed between the anvils flats and the gasket. Temperature was measured with a Pt/Pt-10%Rh thermocouple. Temperatures up to 500 K and pressures up to 3.2 GPa were routinely obtained with this set up.

The calculation technique is a fully self-consistent density functional theory[23] (DFT) method that has been described with detail in Ref. 13. The valence one-particle problem was solved using a linear combination of numerical (pseudo) atomic orbitals (NAO) with finite range.[24] The calculations were performed using the SIESTA code.[25,26] For band structure calculations at high pressures, the pressure dependences of lattice parameters were taken from Ref. 27 (InSe) and Ref. 7 (GaSe) and the atomic positions inside the cell were assumed to be those proposed in Ref. 28 (InSe) and Ref. 29 (GaSe), on the basis of extended x-ray absorption fine struc-

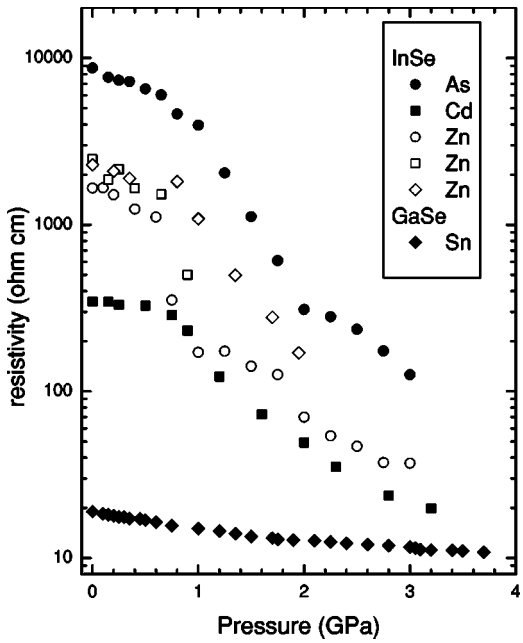

FIG. 1. Resistivity at room temperature as a function of pressure for several *p*-type γ-InSe and ε-GaSe samples with different doping agents.

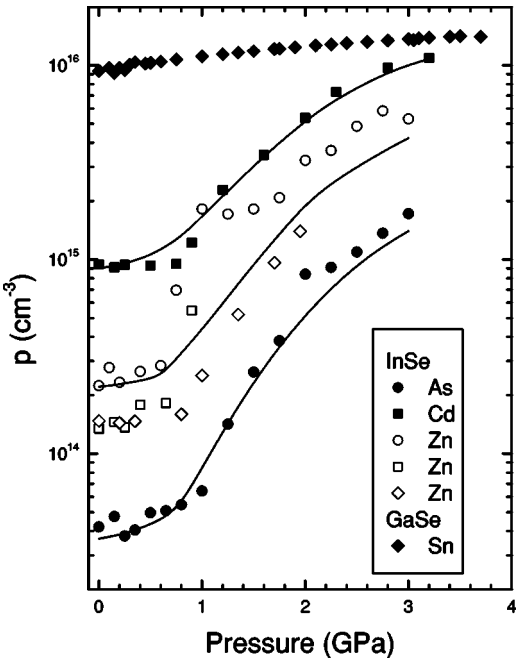

FIG. 2. Hole concentration at room temperature as a function of pressure for several *p*-type γ-InSe and ε-GaSe samples with different doping agents.

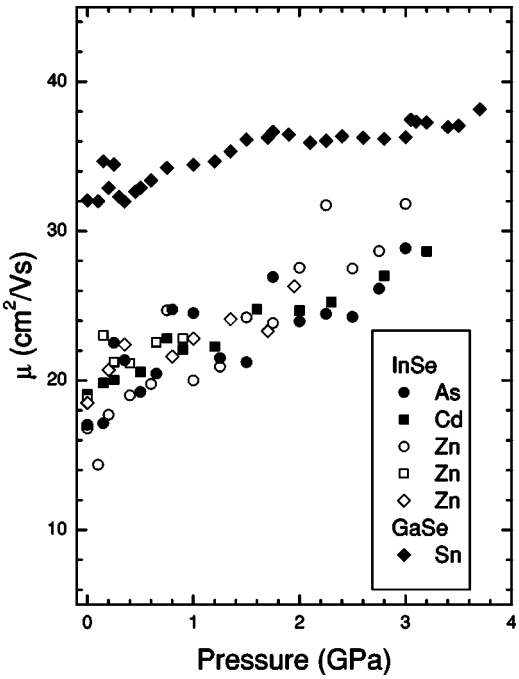

FIG. 3. Hole Hall mobility at room temperature as a function of pressure for several *p*-type γ-InSe and ε-GaSe samples with different doping agents.

TABLE I. Transport parameters of selected *p*-type InSe samples as obtained from Hall effect and resistivity measurements at ambient conditions and impurity concentration of the selected samples. The ambient condition ionization energy of the deep donor and the mobility of the holes located at the *Z* (*RS*) maximum as well as the acceptor and deep donor concentration are also given.

Sample	ρ_0 (Ω cm)	p_0 (cm^{-3})	μ_0 ($cm^2/V\,s$)	μ_{Z0} ($cm^2/V\,s$)	μ_{RS0} ($cm^2/V\,s$)	μ_{RS0}/μ_{Z0}	N_A (cm^{-3})	N_T-N_A (cm^{-3})	E_{T0} (meV)
1.3 ppm As	8700	4.2×10^{13}	17.0	16.0	22.0	1.37	1×10^{18}	5×10^{16}	490
0.93% Cd	350	9.4×10^{14}	19.0	18.0	21.5	1.20	6.1×10^{18}	2×10^{16}	465
1000 ppm Zn	1650	2.2×10^{14}	16.8	15.5	22.5	1.45	2×10^{18}	1×10^{14}	535

ture experiments under pressure. For γ-InSe, the computational details are those reported in Ref. 13. For Ga, norm-conserving scalar non-relativistic pseudopotentials were used. Otherwise, the computational details are those in Ref. 30. In the calculations for ε-GaSe, a cutoff of 660 Ry and a regular grid of $8\times8\times8$ *k* points[31] to sample the Brillouin zone were used.

III. EXPERIMENTAL RESULTS

Figures 1–3 show the resistivity (ρ), hole concentration (p), and hole mobility (μ) as a function of pressure for several samples doped with As, Cd, and Zn, respectively, and a sample of Sn-doped GaSe as representative of results reported in Ref. 19. Table I gives the ambient conditions of resistivity (column 2), hole concentration (column 3), and hole mobility (column 4) for three selected samples as well as their doping agent content. In all the studied samples ρ shows a nearly flat behavior up to 0.8 GPa, but above this pressure an abrupt decrease of ρ is observed. From 0.8 GPa to 3.2 GPa ρ falls more than one order of magnitude. This change of ρ is basically due to the large increase observed in the hole concentration above 0.8 GPa. (See Fig. 2.) In contrast, the hole mobility does not show any abrupt change on the pressure range covered by our studies. Upon compression, it continuously increases doubling its ambient pressure value by 3.2 GPa. This pressure behavior observed for ρ, p,

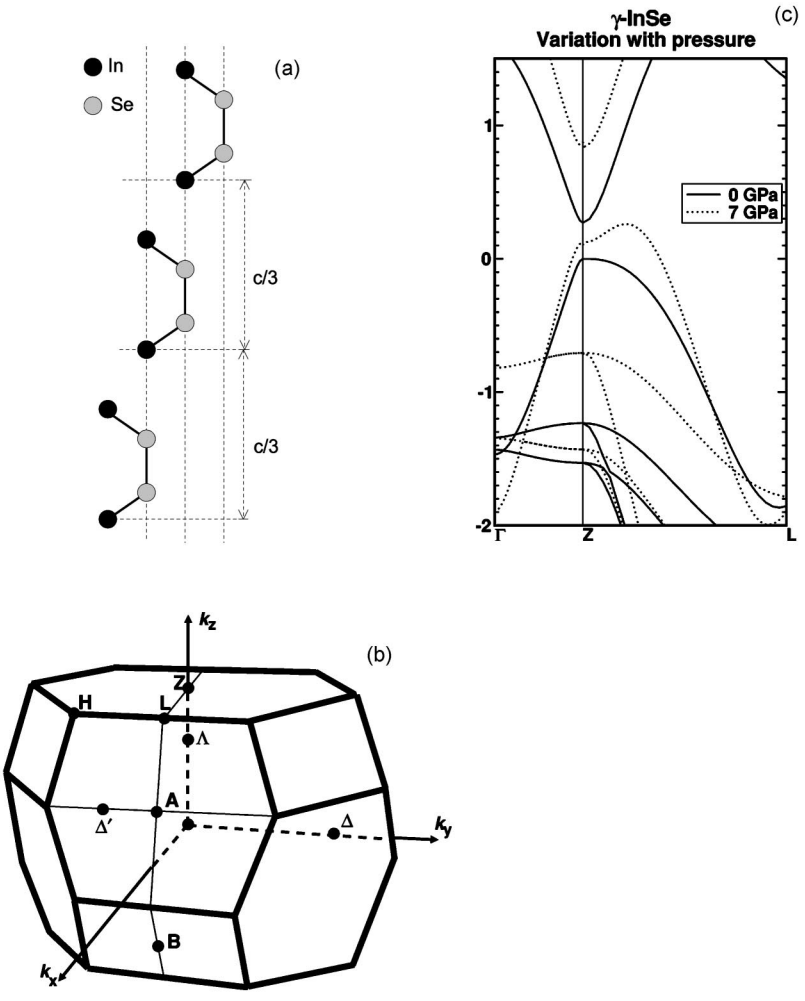

FIG. 4. (a) Projection of the γ-InSe structure in the 110 direction. (b) Brillouin zone of γ-InSe. (c) Band structure of γ-InSe at ambient pressure and 7 GPa as calculated by the NAO-DFT method.

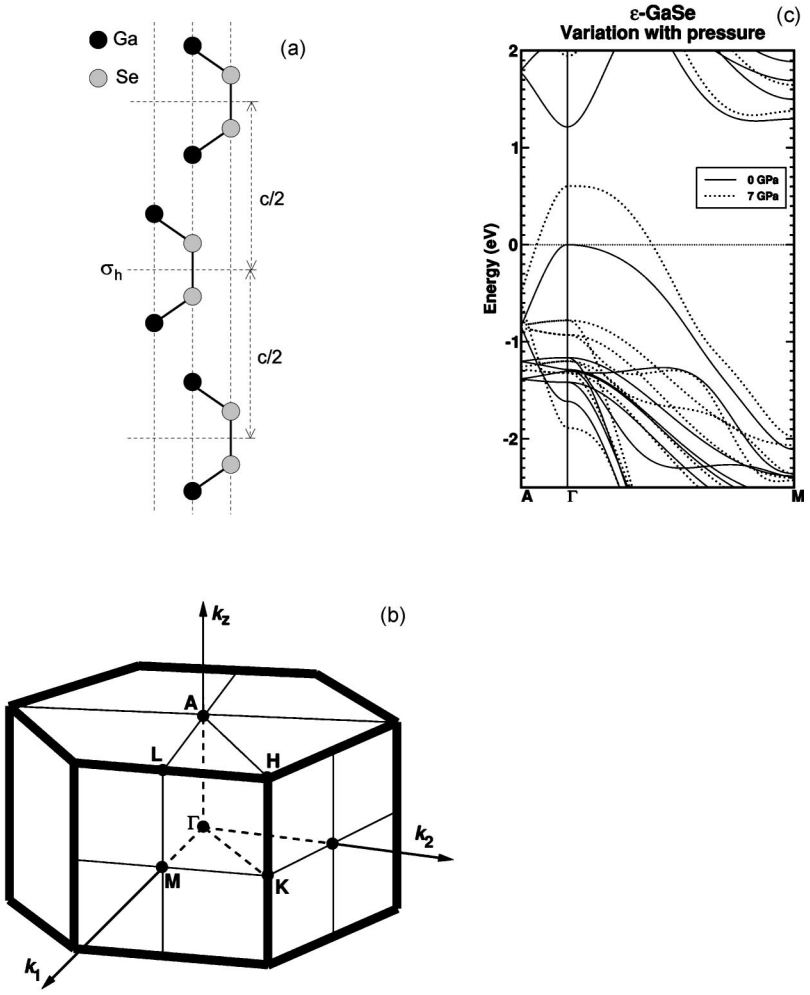

FIG. 5. (a) Projection of the ε-GaSe structure in the 110 direction. (b) Brillouin zone of ε-GaSe. (c) Band structure of ε-GaSe at ambient pressure and 7 GPa as calculated by the NAO-DFT method.

and μ is quite different from the behavior observed in *p*-type GaSe, another III-VI layered semiconductor, as illustrated in Figs. 1–3. In GaSe, from ambient pressure to 4 GPa, p increases only by two times and μ increases by less than 1.2 times. This behavior could be quantitatively explained through a reduction of the activation energy of the acceptor levels and a decrease of the hole-phonon coupling constants[19] as a consequence of the large increase of the static dielectric constant in the direction parallel to the *c* axis.[32,33] Nevertheless, such smooth changes can hardly be expected to cause the large increase observed in the transport parameters of *p*-type InSe under compression. In fact, the observed pressure behavior for the transport properties of *p*-type InSe can be only understood on the basis of a sizable increase of the valence band density of states accompanied by a decrease of the effective mass in the valence band maximum. As we will show below, these conditions can be accounted for if the band structure is modified under compression in the way predicted by DFT calculations.[13,14]

IV. DISCUSSION: EVOLUTION OF THE BAND STRUCTURE UNDER PRESSURE

Figures 4 and 5 show the evolution of the band structure of γ-InSe and ε-GaSe near the band gap at two different pressures (ambient pressure and 7 GPa) along two directions of the Brillouin zone (BZ) as calculated by the NAO-DFT method.[25,26] Apart from the band gap value, the band structure of ε-GaSe at ambient pressure can be seen as the result of the folding of the band structure of γ-InSe along the Γ-Z direction. Let us call E_{Vi} the energy of the i valence band at $Z(\Gamma)$ in InSe (GaSe), i.e., E_{V1} correspond to the valence

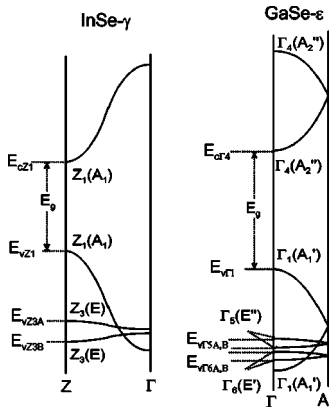

FIG. 6. Comparison of the band structures of γ-InSe and ε-GaSe at ambient pressure with assignment of the symmetry of each state at the Z or Γ points of the BZ.

TABLE II. Selection rules in III-VI polytypes. (a) ε-polytype (D_{3h}). (b) γ-polytype (C_{3v}).

	Final state	
Initial state	$E \perp c$[a]	$E \parallel c$[a]
Γ_1 (A_1')	Γ_6	Γ_4
Γ_4 (A_2'')	Γ_5	Γ_1
Γ_5 (E'')	Γ_4, Γ_5	Γ_6
Γ_6 (E')	Γ_1, Γ_6	Γ_5
	$E \perp c$[b]	$E \parallel c$[b]
Z_1 (A_1)	Z_3	Z_1
Z_3 (E)	Z_1, Z_3	Z_3

[a]Dipole operator has $\Gamma_6(E')$ symmetry for $E \perp c$ and $\Gamma_4(A_2'')$ for $E \parallel c$.
[b]Dipole operator has $Z_3(E)$ symmetry for $E \perp c$ and $Z_1(A_1)$ for $E \parallel c$.

band maximum (VBM). As discussed in the literature,[7,10,13] the upper valence band with energy E_{V1} has predominant Se-p_z character in both compounds, while the following deeper valence bands have predominant Se-p_x-p_y character. These deeper valence bands are at energies E_{Vi} ($i=2$ and $i=3$) in InSe and E_{Vi} ($i=2$ to $i=5$) in GaSe. As pressure increases, two striking differences become more and more apparent in the valence bands of both compounds.

(i) On the one hand, there is a clearly different behavior in the change of the valence band maximum (VBM). While the VBM in ε-GaSe does not change its shape as pressure increases, the VBM of γ-InSe at Z first becomes very flat and then, at a higher pressure, a second maximum develops in the Z-L direction of the BZ. A detailed analysis shows that this maximum has quasicylindrical symmetry with respect to the c axis and its constant energy surface is ring-shaped (detailed cross sections of the constant energy surfaces are shown in Ref. 14). At pressures larger than 3 GPa, this second maximum becomes the absolute maximum.

(ii) On the other hand, there is a second difference regarding the behavior of the energy difference between the VBM and the deeper valence bands. While in ε-GaSe the energy difference $E_{V1}-E_{Vi}$ monotonously increases with pressure for all deeper valence bands ($i=2$ to $i=5$), it decreases in γ-InSe for $i=2$, and increases for $i=3$.

Let us first try to understand the origin of these differences. Figure 6 shows a sketch of the band structure of both compounds in the Γ-Z (Γ-A) direction of InSe (GaSe), with the assignment of the symmetry of the electronic states in the $Z(\Gamma)$ point of the BZ. Table II shows the selection rules for dipole transitions in both point groups (C_{3v} for γ-InSe and D_{3h} for ε-GaSe).

A. Anisotropy of the valence band maximum

For both semiconductors and in the absence of spin-orbit interaction, the fundamental transition is forbidden for light polarization perpendicular to the c axis ($E \perp c$) and allowed for light polarization parallel to the c axis ($E \parallel c$). Then, in the framework of the $\vec{k}\cdot\vec{p}$ model,[34] the hole effective mass parallel to the c axis would be determined mainly by the dipole matrix element of the allowed fundamental transition. (In the following see Fig. 6 for the notation of bands and their corresponding energies.)

$$\left[\frac{m_0}{m_{\nu Z}}\right]_{\parallel}^{(InSe)} = 1 - \frac{2}{m_0}\frac{|\langle \nu Z_1|P_{\parallel}|cZ_1\rangle|^2}{E_{g,InSe}}, \tag{1}$$

$$\left[\frac{m_0}{m_{\nu Z}}\right]_{\parallel}^{(GaSe)} = 1 - \frac{2}{m_0}\frac{|\langle \nu \Gamma_1|P_{\parallel}|c\Gamma_4\rangle|^2}{E_{g,GaSe}}. \tag{2}$$

As the matrix elements in Eqs. (1) and (2) are very large, the negative term dominates, giving rise to a small hole effective mass and, consequently, to a large dispersion of the VBM along the c-axis direction. (See Figs. 4 and 5.)

As the fundamental transition is forbidden for light polarization perpendicular to the c axis, the hole effective mass in the layer plane is determined by other allowed transitions from the VBM to other valence and conduction bands. (See Table II.)

$$\left[\frac{m_0}{m_{\nu Z}}\right]_{\perp}^{(InSe)} = 1 - \frac{2}{m_0}\frac{|\langle \nu Z_1|P_{\perp}|cZ_3\rangle|^2}{E_{cZ3}-E_{\nu Z1}} + \frac{2}{m_0}\frac{|\langle \nu Z_1|P_{\perp}|\nu Z_{3A}\rangle|^2}{E_{\nu Z1}-E_{\nu Z3A}} + \frac{2}{m_0}\frac{|\langle \nu Z_1|P_{\perp}|\nu Z_{3B}\rangle|^2}{E_{\nu Z1}-E_{\nu Z3B}}, \tag{3}$$

$$\left[\frac{m_0}{m_{\nu \Gamma 1}}\right]_{\perp}^{(GaSe)} = 1 - \frac{2}{m_0}\frac{|\langle \nu \Gamma_1|P_{\perp}|c\Gamma_6\rangle|^2}{E_{c\Gamma 6}-E_{\nu \Gamma 1}} + \frac{2}{m_0}\frac{|\langle \nu \Gamma_1|P_{\perp}|\nu \Gamma_{6A}\rangle|^2}{E_{\nu \Gamma 1}-E_{\nu \Gamma 6A}} + \frac{2}{m_0}\frac{|\langle \nu \Gamma_1|P_{\perp}|\nu \Gamma_{6B}\rangle|^2}{E_{\nu \Gamma 1}-E_{\nu \Gamma 6B}}. \tag{4}$$

The second right-hand term in Eqs. (3) and (4) corresponds to the dipole-allowed interaction with conduction bands (with In p_x-p_y character) lying 5–6 eV above the VBM. The third and fourth terms correspond to dipole-allowed interaction with valence bands with Se p_x-p_y character. Then, for both materials, the positive terms partially compensate the negative ones, which leads to a large value of the in-plane hole effective mass. Consequently, selection rules for the fundamental transition give full account, following the $\vec{k}\cdot\vec{p}$ model, of the so-called "anomalous anisotropy" of the hole effective mass in both materials. (The hole effective mass component parallel to the c axis is much smaller than the ones perpendicular to it, $m_{\parallel}^{*} \ll m_{\perp}^{*}$, as clearly illustrated by the band dispersion in Figs. 4 and 5.)

B. Emergence of the ring-shaped maximum

In order to explain the emergence of the ring-shaped VBM in γ-InSe, following the model proposed in Ref. 14, Eq. (3) is modified as follows:

$$\left[\frac{m_0}{m_{\nu Z}}\right]_{\perp}(k_{\perp}) = 1 + \frac{2}{m_0}\left(-\frac{|\langle \nu Z_1|P_{\perp}|cZ_3\rangle|^2}{E_{cZ3}-E_{\nu Z1}} - (A+Bk_{\perp}^2)^2 \times \frac{|\langle \nu Z_3|P_{\perp}|cZ_1\rangle|^2}{E_g} + \frac{|\langle \nu Z_1|P_{\perp}|\nu Z_{3A}\rangle|^2}{E_{\nu Z1}-E_{\nu Z3A}} + \frac{|\langle \nu Z_1|P_{\perp}|\nu Z_{3B}\rangle|^2}{E_{\nu Z1}-E_{\nu Z3B}}\right). \quad (5)$$

The new term gives account of a small dipole-allowed interaction with the Z_1 conduction band minimum, arising from Z_1 and Z_3 valence band mixing of two different origins. Coefficient A describes the spin-orbit interaction at Z and the $k_{\perp}$-dependent term describes the mixing of states away from the c axis.

As pressure increases, the energy difference $E_{\nu Z1}-E_{\nu Z3A}$ quickly decreases and the fourth term becomes dominant, compensating for the negative ones and giving rise to an upward dispersion of the VB at $Z(k_{\perp}=0)$. For $k_{\perp}\neq 0$, the terms in $k_{\perp}^2$ in the third term dominate for some given value of $k_{\perp}$ and dispersion becomes downward, which leads to the emergence of the ring-shaped maximum.

Let us now discuss what happens in ε-GaSe under pressure. Equation (4) is also modified in order to introduce dipole interaction associated to the fundamental gap,

$$\left[\frac{m_0}{m_{\nu\Gamma 1}}\right]_{\perp}(k_{\perp}) = 1 - \frac{2}{m_0}\left(\frac{|\langle \nu\Gamma_1|P_{\perp}|c\Gamma_6\rangle|^2}{E_{c\Gamma 6}-E_{\nu\Gamma 1}} - (A+Bk_{\perp}^2)^2 \times \frac{|\langle \nu\Gamma_5|P_{\perp}|c\Gamma_4\rangle|^2}{E_g} + \frac{|\langle \nu\Gamma_1|P_{\perp}|\nu\Gamma_{6A}\rangle|^2}{E_{\nu\Gamma 1}-E_{\nu\Gamma 6A}} + \frac{|\langle \nu\Gamma_1|P_{\perp}|\nu\Gamma_{6B}\rangle|^2}{E_{\nu\Gamma 1}-E_{\nu\Gamma 6B}}\right). \quad (6)$$

Contrary to what happens in γ-InSe, terms giving rise to positive contributions to the hole effective mass decrease under pressure in ε-GaSe, as the energy differences $E_{\nu\Gamma 1}-E_{\nu\Gamma 6A,B}$ quickly increase. (See Fig. 5.) Consequently, no change of the VBM shape is expected in ε-GaSe under pressure. This is fully coherent with band structure calculations (see Fig. 5) and also with the monotonous change of all hole transport parameters in GaSe, as shown in Figs. 1–3 that could be quantitatively interpreted in Ref. 19 by taking into account smooth changes of physical quantities like the static dielectric constant, effective mass, phonon frequencies, etc.

C. Selection rules in the isolated layer and dipole matrix elements in the crystals

A comparison of Eqs. (5) and (6), in light of the selection rules for both polytypes (Table II) can bring more light, especially on which concerns the order of magnitude of the matrix elements in γ-InSe. In order to compare γ and ε polytypes in III-VI layered semiconductors one has to consider the electronic structure of an isolated layer and the effect that the different stacking sequences have on it. The symmetry point group of the isolated layer is D_{3h}, which contains the mirror plane σ_h, perpendicular to the c axis. This symmetry, along with the bonding scheme, determines the chemical nature and the basic in-layer structure of the electronic wave functions. In the ε-polytype the symmetry and selection rules of the single layer are preserved in the 3D crystal. In the γ-polytype the stacking sequence breaks the σ_h mirror plane symmetry. Nevertheless, given the much smaller strength of interlayer interactions with respect to intra-layer bonding, one cannot expect a dramatic change of the intralayer structure of electronic wave functions. It means that, in spite of a given transition being allowed by the crystal symmetry in the γ-polytype, its matrix element can be very small. In some way, the 3D crystal wave functions preserve the "print" of the σ_h mirror plane in the isolated layer. This has been shown to be the case for the vZ_{3B}-cZ_1 transition in γ-InSe. Dielectric function calculations reported in Ref. 14 show that, even if this transition is allowed for $E\perp c$, it does not contribute to the dielectric constant because the matrix element is negligible. This is a "print" of the fact that the corresponding transition is strictly forbidden in the isolated layer (as well as in the ε-polytype). It is reasonable to think that this is also the case of the vZ_{3A}-vZ_1 transition in γ-InSe that corresponds to strictly forbidden transitions $v\Gamma_{5A,B}$-$v\Gamma_1$ in ε-GaSe. Its matrix element $\langle \nu Z_1|P_{\perp}|\nu Z_{3A}\rangle$ is small and it does not give any large positive contribution in Eq. (1) at ambient pressure. On these grounds, it turns out that Eq. (6) can give account for the complex structure of the VBM near Z, depending on the relative value of the different matrix elements and depending on the relative value and signs of coefficients A and B. As regards the signs of these coefficients, energy dispersion considerations suggest that A and B should have different signs. On the one side, A describes the mixing of states with double-group symmetry $Z_6(J=1/2)$ and should contribute with an upward shift of the VBM (repulsion or anticrossing as shown in Ref. 18). On the other side, B describes the strong mixing of p_z and p_x-p_y Se states away from the Z point that is responsible for most of the downward dispersion of the upper valence band in the layer plane.

Let us now consider the effect of compression on the value of the matrix elements. The main effect of compression in layered semiconductors is the quick decrease of the interlayer distances. In the γ-polytype, this can affect the print of the σ_h symmetry in two ways; on the one hand, it increases the intra-layer dissymmetry with respect to the mirror plane[18] and, on the other hand, it makes the influence of the nonsymmetric interlayer space on the electronic wave functions become larger under pressure. Consequently, a matrix element that was zero in the isolated layer and negligible in the 3D crystal at ambient pressure can quickly increase under pressure. This effect, along with the quick decrease of the energy $E_{\nu Z1}-E_{\nu Z3A}$ eventually leads to a change of sign of the curvature of the VBM at Z and the emergence of the ring-shaped new VBM.

D. On the origin of the pressure behavior of the transition energies

Another important point in this model is the reason why the energy difference $E_{\nu Z1}-E_{\nu Z3A}$ decreases in InSe while all the energy differences $E_{\nu\Gamma 1}-E_{\nu\Gamma 5,6,A,B}$ increase in GaSe. This can be hardly related to the polytype symmetry as in both

polytypes the states involved in each transition under consideration belong to different representations and do not mix under pressure. We think that the origin of the different behavior can hold on two grounds: (i) the compressibility of the cation-cation bond length that is responsible for the energy splitting of the Se p_x-p_y states. (For symmetry reasons, the coupling between Se p_x-p_y states operates mainly through their interaction with the In p_x-p_y states.) and (ii) the relative strength of interlayer and intralayer interactions in both compounds, along with the Se p_z nature of the VBM.

As regards the first ground, it turns out that the In-In bond is more compressible than the Ga-Ga one, which leads to a quicker increase of the splitting between the Se p_x-p_y states, making the "antibonding" Se p_x-p_y state in InSe ($v Z_{3A}$) shift up in energy quicker than the equivalent pair in GaSe ($v\Gamma_{5A,B}$). The upper Z_{3A} Se p_x-p_y state at Z in γ-InSe shifts up in energy by 0.52 eV between ambient pressure (AP) and 7 GPa. The corresponding state at Γ in ε-GaSe (Γ_{5A}) shifts up only by 0.37 eV in the same pressure interval.

As regards the second ground, the VB states with Se p_z character are very sensitive to the increase of the interlayer interaction under pressure. From Figs. 4 and 5 it is clear that the increase of the band dispersion of these states in GaSe ($v\Gamma_1$) increases quicker than the equivalent states in InSe (vZ_1). This behavior reflects the fact that intralayer interaction in GaSe is relatively much more intense (with respect to the interlayer interaction) than it is in InSe. (Intralayer covalent bonds are stronger and intralayer distances are longer in GaSe with respect to InSe.) Under compression, interlayer interaction can increase more in GaSe than it does in InSe, which makes the upper energy shift of $v\Gamma_1$ in GaSe (0.6 eV from 1 bar to 7 GPa) to be much quicker than the one of vZ_1 in InSe (0.12 eV from 1 bar to 7 GPa).

V. INTERPRETATION OF THE PRESSURE BEHAVIOR OF HOLE TRANSPORT PARAMETERS IN γ-InSe

For convenience, we will call the two maxima of the valence band, Z maximum and *RS* (ring-shaped) maximum. The energy difference between the Z and *RS* maxima[13] is at any pressure much smaller that the activation energy of the hole traps that determine the hole concentration of p-type InSe.[20] As a consequence of this fact, holes at the Z and *RS* maxima will be involved in the charge transport process. It is important to note here that our electronic structure calculations show a continuous change in the shape of the valence band. According to this, the effective mass tensor at Z should have two components that are infinite at some pressure before becoming negative. (Above that pressure the VBM at Z would become a saddle point.) We think that this is unrealistic result due to the limitations of the band structure calculations (which do not include spin-orbit interaction). Once spin-orbit interaction is taken into account, Eq. (6) can give account of a complex structure of the VBM around Z, with a conventional maximum at Z and a ring-shaped maximum away from Z. On the other side, all results on absorption,[13,35] modulated photoreflectance,[36] and photoluminescence[37] under compression exclude the existence of a saddle point. In particular, the monotone and relatively small change of the exciton effective Rydberg under pressure, as measured from the absorption edge at low temperature[35] would be incompatible with the existence of a saddle point at the Z point. On top of that, a change of sign in the curvature of the VBM at Z would also have very dramatic effects on the hole mobility. The VBM would become very flat at a given pressure and the hole effective mass parallel to the layers would become very large, leading to a very large density of states and a very low hole mobility. None of these effects seem to be compatible with the results of our transport measurements. Then assuming that we have two distinct types of carriers is an assumption coherent with optical measurements. Within this framework, the Hall hole concentration and mobility will be given by[15,16]

$$p = \frac{(p_{RS}\mu_{RS} + p_Z\mu_Z)^2}{p_{RS}\mu_{RS}^2 + p_Z\mu_Z^2}, \tag{7}$$

and

$$\mu = \frac{p_{RS}\mu_{RS}^2 + p_Z\mu_Z^2}{p_{RS}\mu_{RS} + p_Z\mu_Z}, \tag{8}$$

respectively, where p_Z (p_{RS}) represents the hole electron concentration at the Z (*RS*) maximum of the valence band, and μ_Z (μ_{RS}) stands for the mobility of the hole located at the Z (*RS*) maximum of the valence band. On the other hand, it has been established by previous studies that doping with As, Cd, and Zn create shallow acceptors and deep donors in InSe.[20] These donors are located below the middle of the band gap and behave as hole traps so that the Fermi level is nearer to the valence band than to the conduction band and the electron concentration can be neglected in the neutrality equation. On top of that, in contrast with the p-type GaSe samples, in the p-type InSe samples used to perform the present measurements, the acceptor levels are fully ionized, as established in Ref. 20. These samples are overcompensated by very deep donors and holes are generated by excitation from the valence band to the empty deep donors. We do not observe any departure from this behavior in the whole pressure and temperature range we have explored. With these assumptions p_Z and p_{RS} will be related through the following equation,

$$\frac{p_{RS}}{p_Z} = \frac{N_{VRS}}{N_{VZ}} e^{(E_Z - E_{RS})/k_B T}, \tag{9}$$

where k_B is the Boltzmann constant, E_Z (E_{RS}) are the energies of the Z (*RS*) VBM and N_{VZ} (N_{VRS}) are the effective density of states in these maxima, given by

$$N_{VZ} = 4.89 \times 10^{15} T^{3/2} (m_Z^*/m_0)^{3/2}\ \text{cm}^{-3}, \tag{10}$$

$$N_{VRS} = k_B T \frac{m_{RS}^* k_{RS}}{\pi \hbar^2}, \tag{11}$$

where m_0 is the free electron mass, m_Z^* is the density of states effective mass in the Z-VBM, m_{RS}^* is the density of states effective mass in the *RS*-VBM, and k_{RS} is the radius of the ring central circumference of the *RS* maximum. (See the Appendix.) From Eqs. (9)–(11), and using the hole statistics

TABLE III. Calculated values for m_Z^*, m_{RS}^*, μ_Z, and μ_{RS} as a function of pressure. The estimated pressure dependence for the energy difference between the *Z* and *RS* maxima and the pressure dependence of E_T obtained from Fig. 8 are also given.

P (GPa)	E_T (meV)	$E_Z - E_{RS}$ (meV)	m_Z^*/m_0	m_{RS}^*/m_0	μ_Z (cm^2/V s)	μ_{RS} (cm^2/V s)
0.0	465[a]	70.0	0.449	0.350	18.0	21.5
0.75	454[b]	53.5	0.420	0.356	20.16	24.09
1.2	444[b]	43.6	0.435	0.360	21.23	25.36
1.8	426[b]	30.4	0.492	0.366	23.4	26.76
2.4	420[b]	17.2	0.586	0.371	23.32	27.86
3.2	414[c]	−0.4	0.755	0.378	24.25	28.93

[a]Value taken from Ref. 20.
[b]Values obtained from our measurements.
[c]Extrapolated value.

model described in Ref. 20 it is straightforward to obtain the hole concentrations in each maximum,

$$p_Z = N_{VZ}\alpha\left(1+\frac{N_T-N_A}{2N_V\alpha}\right)\left[\sqrt{1+\frac{2N_A}{N_V\alpha}\left(1+\frac{N_T-N_A}{2N_V\alpha}\right)^{-2}}-1\right], \tag{12}$$

and

$$p_{RS} = p_Z\left(\frac{N_V}{N_{RS}}-1\right), \tag{13}$$

where N_A is the acceptor concentration, N_T is the deep donor concentration, and $\alpha=\exp[(E_T-E_Z)/k_BT]$, E_T is the energy of the deep donor and

$$N_V = N_{VZ} + K_BT(m_{RS}^* k_{RS}/\pi\hbar^2)\exp[(E_Z-E_{RS})/K_BT]. \tag{14}$$

In order to calculate the pressure dependence of transport parameters of the studied samples using Eqs. (7)–(13) it is necessary to know N_A, N_T, E_T, and the pressure dependence of the hole effective masses (m_Z^* and m_{RS}^*), the energy difference between the *Z* and *RS* maxima (E_Z-E_{RS}), and the hole mobilities (μ_Z and μ_{RS}). N_A, N_T, E_T, and the pressure dependence of E_Z-E_{RS} can be taken from the literature.[13,20] For m_Z^*, its pressure dependence can be calculated using the modified $\vec{k}\cdot\vec{p}$ model proposed by Manjón,[38] and, for m_{RS}^*, its pressure dependence can be obtained from DFT calculations.[13] Regarding μ_Z, it can be accounted for by including LO polar phonon, homopolar phonon, and ionized impurity scattering.[19,39] On the other hand, it is reasonable to assume that μ_Z and μ_{RS} have the same pressure dependence within the range of the present study.[16] Thus, in order to fit the experimental behavior of p and μ we assumed that μ_Z and μ_{RS} follow the pressure dependence calculated in Ref. 19, being its ambient pressure value fitting parameters. It is important to note here that the ambient pressure values of the hole mobilities are the only two fitting parameters we have used to calculate the transport parameters; the rest of the parameters involved in Eqs. (7)–(9) and their pressure dependences were obtained from previous experiments and calculations. All the parameters used to calculate the pressure dependence of the hole concentration and mobility are summarized in Tables I and III.

Before proceeding with the discussion one word should be said on the hole trap activation energy. We first tried to account for the experimental results by considering E_T as a constant. In such a case, we obtained that p increases upon compression, but not as much as observed in the experiments, e.g., in the Cd-doped sample p goes from 10^{15} cm^{-3} at ambient pressure to 4×10^{15} cm^{-3} at 3 GPa which is much lower than the experimental value at 3 GPa ($p=9\times10^{15}$ cm^{-3}). Therefore, the E_T constant approach does not allow us to estimate properly the pressure dependence of p as

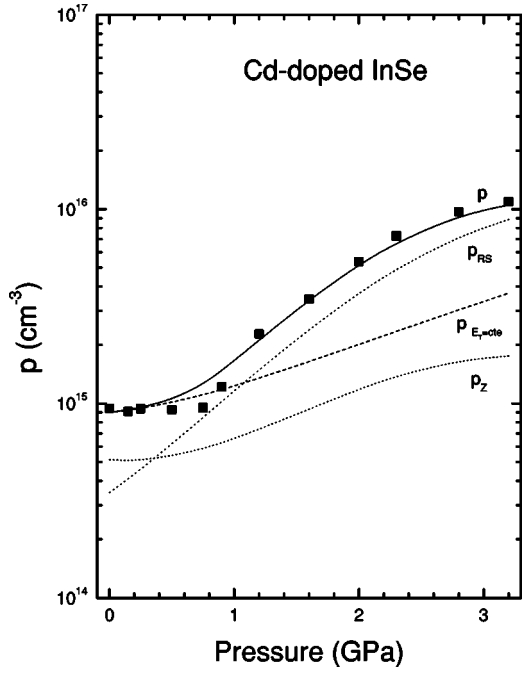

FIG. 7. Pressure dependence of the hole concentration for the sample of γ-InSe-doped with Cd. The symbols show the present experimental data. The solid line represents the calculated pressure behavior of the hole concentration according to the model described in the text. The dotted lines are the calculated p_Z and p_{RS} using Eqs. (12) and (13). The dashed line represents the results obtained considering E_T as pressure independent.

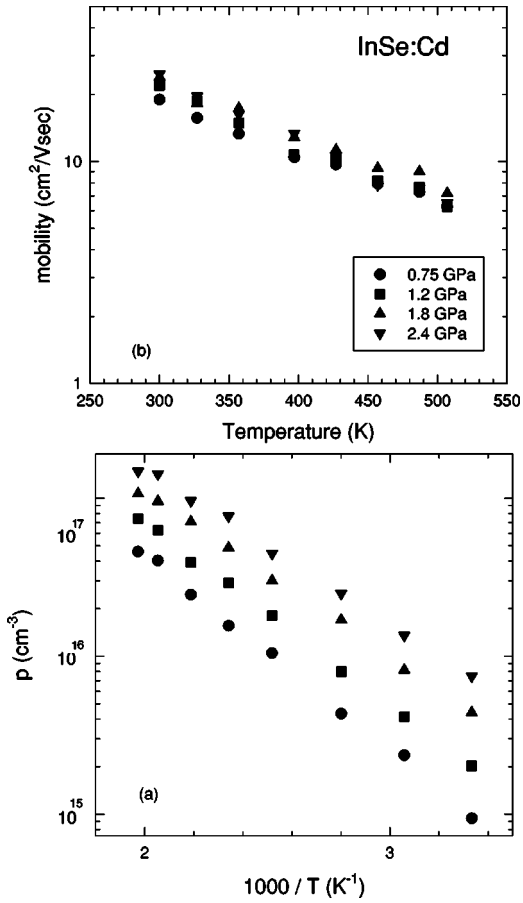

FIG. 8. Temperature dependence of the carrier concentration (a) and mobility (b) at different pressures in the sample of γ-InSe doped with Cd. Different symbols correspond for different pressures, which are indicated in the inset of the figure. The temperature dependence of the mobility does not change with pressure within the accuracy of the present experiments. From the slope change induced by pressure in the Arrhenius plot (a) we obtained the pressure dependence of E_T.

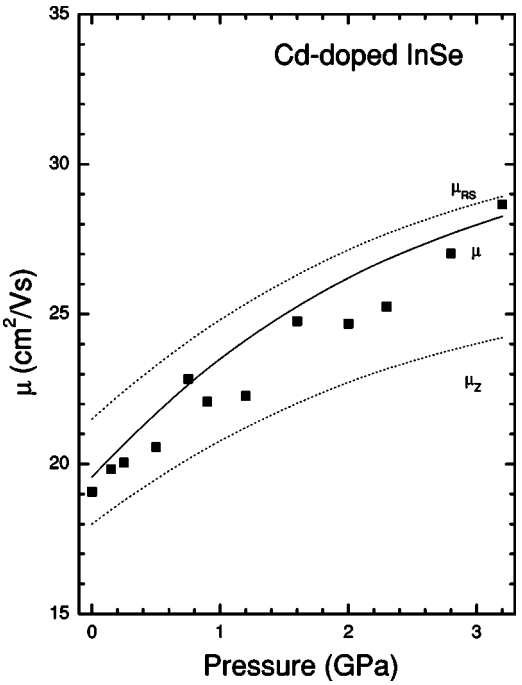

FIG. 9. Hole mobility as a function of pressure for the Cd-doped sample of γ-InSe. The solid squares illustrate the present experimental data. The solid line represents the fitted behavior of μ using Eq. (8). The dashed lines are the mobility of the holes located in the Z maximum (μ_Z) and the RS maximum (μ_{RS}).

illustrated in Fig. 7 for the Cd-doped sample. (The dashed line represents the hole concentration obtained under this approximation.) In order to check whether E_T changes on pressure or not, we performed HE measurements as a function of T at several pressures. The results obtained are shown in Figs. 8(a) and 8(b). In the Arrhenius plot [Fig. 8(a)] it can be seen that the slope decreases at the pressure increases, which implies a decrease of the activation energy of the hole concentration. The values obtained for E_T at different pressures are given in Table III. The pressure behavior we found for E_T is very similar to the one estimated for the activation energy of deep levels in Sn-doped p-type GaSe.[19] Based upon this fact, we assumed that the energy of As and Zn deep levels follows also the same trend. With respect to μ, at all the studied pressures it depends on T in the form $T^{-2.2}$. This dependence is very similar to that observed at ambient pressure[20] and indicates that the contribution of the different scattering mechanisms does not change substantially with pressure.

The results obtained for the hole concentration are shown in Fig. 2 (solid lines). It can be seen there that the present model reproduces well the experimental results for the samples doped with As, Cd, and Zn. To illustrate the fact that the pressure-driven changes of p and μ are related to the changes of the valance band structure predicted by DFT calculations[13] we plotted also in Fig. 7 p, p_Z, and p_{RS} (solid and dotted lines, respectively). The presence of the ring-shaped maximum, which approaches the Z maximum under compression, is reflected in Fig. 7 in the large increase of p_{RS}, which by 1 GPa already exceeds p_Z. On the other hand, as the effective mass of the holes located at the ring-shaped maximum is smaller than the effective mass of the holes at the Z maximum, it is reasonable to expect that $\mu_Z < \mu_{RS}$. Therefore the Hall mobility should increase as the holes are transferred from the Z to the RS maximum due to the pressure-driven valence band modification of InSe. This fact is illustrated in Fig. 9, where it can be clearly seen that $\mu \simeq \mu_Z$ at ambient pressure, but $\mu \simeq \mu_{RS}$ at 3 GPa. Table III shows the best fit values for μ_Z and μ_{RS} at ambient pressure (μ_{Z0} and μ_{RS0}) in the samples doped with As, Cd, and Zn. In all the cases, the mobility ratio μ_{RS0}/μ_{Z0} is very similar to $(m^*_{RS}/m^*_Z)^{-3/2}$ implying that, as in p-type GaSe,[19] the homopolar phonon scattering mechanism is the dominant scattering mechanism in p-type InSe in the pressure range covered by our experiments.

VI. CONCLUSIONS

In this work we have reported transport measurements under pressure in p-type InSe and GaSe. The results obtained from these measurements can be satisfactorily explained if

DFT electronic structure calculations of both compounds are taken into account. In this sense, the differences found in the electronic structure calculations for both compounds and the addition of extra terms related to spin-orbit interaction (not considered in the calculations) have led to equations for the hole effective masses at the topmost valence bands of these compounds. Furthermore, the new equations for the hole effective masses allow us to understand not only the present transport measurements but also previous results of absorption and photoluminescence under pressure in these compounds. We can conclude that transport measurements under pressure, in light of those calculations, turn out to be appropriate tools to compare the different behavior under pressure of the valence band maximum in two closely related compounds with different crystal symmetry.

ACKNOWLEDGMENTS

This study was supported by the Spanish government MCYT under Grant Nos. MAT2002-04539-CO2-01, MAT2002-04539-CO2-02, BFM2003-03372-C03, BFM2001-3309-C02-02, and MAT2004-05867-CO3-01. D.E. thanks the financial support from the MCYT and the University of Valencia through the "Ramón y Cajal" program. The computations described in this work were carried out using the resources of CESCA and CEPBA coordinated by C4. G.T. acknowledges support from Ministerio de Ciencia y Tecnologia of Spain.

APPENDIX: DENSITY OF STATES AND CARRIER STATISTICS IN A RING-SHAPED (TOROIDAL) EXTREMUM

Let us assume for simplicity that the ring-shaped (toroidal) extremum occurs in the $k_z=0$ plane and has cylindrical symmetry with respect to the k_z axis. Let us call k_{RS} the radius of the central circumference of the toroid. Let us assume that the constant energy surface intersection with planes containing the k_z axis are also circumferences (i.e., the effective mass is the same for $\vec{k}$ parallel or perpendicular to the c axis). Under these assumptions the energy dispersion for k vectors close to the $k_\perp = k_{RS}$ circumference will be

$$E(\vec{k}) = E_{RS} - \frac{\hbar^2}{2m^*}|\vec{k} - \vec{k}_{RS}|^2 = E_{RS} - \frac{\hbar^2}{2m^*}|\Delta\vec{k}|^2, \quad \text{(A1)}$$

where $\vec{k}_{RS}$ is a vector on the toroid central circumference with the same spherical coordinate φ as $\vec{k}$. In spherical coordinates, Eq. (A1) can be written as

$$E(\vec{k}) = E_{RS} - \frac{\hbar^2}{2m^*}(k^2 + k_{RS}^2 - 2kk_{RS}\sin\theta).$$

The density of states can be calculated through

$$g_{RS}(E) = \frac{1}{4\pi^3}\iint_{E=cte}\frac{dS_\perp}{|\nabla_{\vec{k}}E(\vec{k})|}.$$

The k gradient of the energy dispersion would be

$$\nabla_{\vec{k}}E(\vec{k}) = -\frac{\hbar^2}{m^*}(k - 2k_{RS}\sin\theta)\vec{u}_k + \frac{\hbar^2}{m^*}k_{RS}\cos\theta\vec{u}_\theta,$$

$$|\nabla_{\vec{k}}E(\vec{k})| = \frac{\hbar^2}{m^*}[(k - 2k_{RS}\sin\theta)^2 + (k_{RS}\cos\theta)^2]^{1/2} = \frac{\hbar^2}{m^*}|\Delta\vec{k}|.$$

The surface element on the constant energy surfaces can be easily expressed by using as an angular coordinate the angle δ (angle between $\Delta\vec{k}$ and $\vec{k}_{RS}$),

$$dS_\perp = dk_\varphi dk_\delta = k_{RS}|\Delta\vec{k}|d\varphi d\delta,$$

$$g_{RS}(E) = \frac{1}{4\pi^3}\int_0^{2\pi}\int_0^{2\pi}\frac{k_{RS}|\Delta\vec{k}|}{\frac{\hbar^2}{m_{RS}^*}|\Delta\vec{k}|}d\varphi d\delta = \frac{m_{RS}^* k_{RS}}{\pi\hbar^2}.$$

The density of states in a ring-shaped maximum behaves as the one in a two-dimensional (2D) hole system. (It is zero for $E > E_{RS}$ and constant for $E < E_{RS}$.) In this case, as it is well known, the hole concentration is related to the Fermi level by an analytical expression that is valid for both nondegenerate and degenerate systems,

$$p = k_B T\frac{m_{RS}^* k_{RS}}{\pi\hbar^2}\ln(1 + e^{(E_F - E_{RS})/k_B T}),$$

which, in nondegenerate systems, reduces to

$$p = k_B T\frac{m_{RS}^* k_{RS}}{\pi\hbar^2}e^{(E_F - E_{RS})/k_B T}.$$

*Corresponding author. Email address: daniel.errandonea@uv.es

[1] A. Likforman, D. Carré, J. Etienne, and B. Bachet, Acta Crystallogr., Sect. B: Struct. Crystallogr. Cryst. Chem. **B31**, 1252 (1975).

[2] A. Khun, A. Chevy, and R. Chevalier, Phys. Status Solidi A **31**, 469 (1975).

[3] A. Khun and A. Chevy, Acta Crystallogr., Sect. B: Struct. Crystallogr. Cryst. Chem. **B32**, 983 (1976).

[4] A. Polian, K. Kunc, and A. Khun, Solid State Commun. **19**, 1079 (1976).

[5] C. Carlone, S. Jandl, and H. R. Shanks, Phys. Status Solidi A **103**, 123 (1981).

[6] N. Kuroda, O. Ueno, and Y. Nishina, Phys. Rev. B **35**, 3860 (1987).

[7] M. Gauthier, A. Polian, J. M. Besson, and A. Chevy, Phys. Rev. B **40**, 3837 (1989).

[8] J. Camassel, P. Merle, H. Mathieu, and A. Chevy, Phys. Rev. B **17**, 4718 (1978).

[9] R. Le Toullec, N. Piccioli, and J. C. Chervin, Phys. Rev. B **22**, 6162 (1980).

[10] N. Kuroda, Y. Munakata, and Y. Nishina, Solid State Commun. **33**, 687 (1980).
[11] N. Kuroda, O. Ueno, and Y. Nishina, J. Phys. Soc. Jpn. **55**, 581 (1986).
[12] S. G. Abdullayeva, V. A. Gadjiyev, T. G. Kerimova, and E. Yu. Salayev, Nuovo Cimento Soc. Ital. Fis., B **38** 459 (1977).
[13] F. J. Manjón, D. Errandonea, A. Segura, V. Munoz, G. Tobías, P. Ordejón, and E. Canadell, Phys. Rev. B **63**, 125330 (2001).
[14] A. Segura, F. J. Manjón, D. Errandonea, J. Pellicer-Porres, V. Munoz, G. Tobías, P. Ordejón, E. Canadell, A. San Miguel, and D. Sánchez-Portal, Phys. Status Solidi B **235**, 267 (2003).
[15] D. Errandonea, A. Segura, J. F. Sánchez-Royo, V. Muñoz, P. Grima, A. Chevy, and C. Ulrich, Phys. Rev. B **55**, 16 217 (1997).
[16] D. Errandonea, A. Segura, F. J. Manjón and A. Chevy, Semicond. Sci. Technol. **18**, 241 (2003).
[17] G. Ferlat, H. Xu, V. Timoshevskii, and X. Blase, Phys. Rev. B **66**, 085210 (2002).
[18] D. Olguín, A. Cantarero, C. Ulrich, and K. Syassen, Phys. Status Solidi B **235**, 456 (2003).
[19] D. Errandonea, J. F. Sánchez-Royo, A. Segura, A. Chevy, and L. Roa, High Press. Res. **16**, 13 (1998).
[20] A. Segura, M. C. Martínez-Tomás, B. Marí, A. Casanovas, and A. Chevy, Appl. Phys. A: Solids Surf. **44**, 249 (1987).
[21] A. Chevy, J. Appl. Phys. **56**, 249 (1984), and references therein.
[22] A. K. Badyopadhyay, S. Chatterjee, E. S. R. Gopal, and S. V. Subramanyam, Rev. Sci. Instrum. **52**, 1232 (1981).
[23] P. Hohemberg and W. Kohn, Phys. Rev. **136**, B864 (1964).
[24] O. F. Sankey and D. J. Niklevsly, Phys. Rev. B **40**, 3979 (1989).
[25] D. Sánchez-Portal, P. Ordejón, E. Artacho, and J. M. Soler, Int. J. Quantum Chem. **65**, 453 (1997).
[26] J. M. Soler, E. Artacho, J. D. Gale, A. García, J. Junquera, P. Ordejón, and D. Sánchez-Portal, J. Phys.: Condens. Matter **14**, 2745 (2002).
[27] U. Schwarz, A. R. Goñi, K. Syassen, A. Cantarero, and A. Chevy, High Press. Res. **8**, 396 (1991).
[28] J. Pellicer, A. Segura, V. Muñoz, and A. San Miguel, Phys. Rev. B **60**, 3757 (1999).
[29] J. Pellicer-Porres, A. Segura, Ch. Ferrer, V. Muñoz, A. San Miguel, A. Polian, J. P. Itié, M. Gauthier, and S. Pascarelli, Phys. Rev. B **65**, 174103 (2002).
[30] J. F. Sánchez-Royo, J. Pellicer-Porres, A. Segura, V. Muñoz-Sanjosé, G. Tobías, P. Ordejón, E. Canadell, and Y. Huttel, Phys. Rev. B **65**, 115201 (2002).
[31] J. Monkhorst and J. D. Pack, Phys. Rev. B **13**, 5188 (1976).
[32] D. Errandonea, A. Segura, and A. Chevy, Phys. Status Solidi B **211**, 201 (1999).
[33] D. Errandonea, A. Segura, and A. Chevy, Phys. Rev. B **60**, 15 866 (1999).
[34] E. O. Kane, in *The $k\cdot p$ by Method*, Semiconductors and Semimetals Vol. I, edited by Willardson and Beer (Academic, New York, 1966).
[35] A. R. Goñi, A. Cantarero, U. Schwarz, K. Syassen, and A. Chevy, Phys. Rev. B **45**, 4221 (1992).
[36] C. Ulrich, D. Olguin, A. Cantarero, A. Goñi, K. Syassen, and A. Chevy, Phys. Status Solidi B **221**, 777 (2000).
[37] F. J. Manjón, A. Segura, V. Muñoz, G. Tobias, P. Ordejon, and E. Canadell, Phys. Rev. B **70**, 125201 (2004).
[38] F. J. Manjón, Tesis Doctoral, Universidad de Valencia, 1999.
[39] J. F. Sanchez-Royo, D. Errandonea, A. Segura, L. Roa, and A. Chevy, J. Appl. Phys. **83**, 4750 (1998).